

# Structure-Based Carbon Nanotube Sorting by Sequence-Dependent DNA Assembly

Ming Zheng,<sup>1\*</sup> Anand Jagota,<sup>1</sup> Michael S. Strano,<sup>2</sup>  
 Adelina P. Santos,<sup>3†</sup> Paul Barone,<sup>2</sup> S. Grace Chou,<sup>3</sup>  
 Bruce A. Diner,<sup>1</sup> Mildred S. Dresselhaus,<sup>3</sup> Robert S. Mclean,<sup>1</sup>  
 G. Bibiana Onoa,<sup>1</sup> Georgii G. Samsonidze,<sup>3</sup> Ellen D. Semke,<sup>1</sup>  
 Monica Usrey,<sup>2</sup> Dennis J. Walls<sup>1</sup>

Wrapping of carbon nanotubes (CNTs) by single-stranded DNA (ssDNA) was found to be sequence-dependent. A systematic search of the ssDNA library selected a sequence  $d(GT)_n$ ,  $n = 10$  to 45 that self-assembles into a helical structure around individual nanotubes in such a way that the electrostatics of the DNA-CNT hybrid depends on tube diameter and electronic properties, enabling nanotube separation by anion exchange chromatography. Optical absorption and Raman spectroscopy show that early fractions are enriched in the smaller diameter and metallic tubes, whereas late fractions are enriched in the larger diameter and semiconducting tubes.

CNT separation is an enabling step for many potential applications and fundamental studies that require defined nanotube structures and properties (1–5). CNTs can be classified into two categories on the basis of their electronic structures: metallic and semiconducting tubes. The latter can be further classified by tube diameters, because the band gap of a semiconducting tube, a critical parameter that needs to be controlled for nanoelectronic applications, is inversely proportional to its diameter. Reports in the literature indicate that it is possible to separate metallic from semiconducting tubes by taking advantage of differences in their physical or chemical properties (6–8). Diameter-based separation is more difficult, because differences in the physical and/or chemical properties caused by diameter changes are smaller and because variations in tube length could be a dominant factor in physical-based separation methods (9–11). Here, we report our discovery of an oligonucleotide sequence that self-assembles into a highly ordered structure on CNTs, allowing not only markedly improved metal from semiconducting tube separation but also diameter-dependent separation.

We have previously reported that single-stranded DNA (ssDNA) interacts strongly with CNTs to form a stable DNA-CNT hybrid that effectively disperses CNTs in aqueous solution

(6). One important issue not addressed previously is whether or not DNA wrapping on a CNT is dependent on the specific sequence of the DNA strand. Here, we found that anion exchange chromatography provides a macroscopic means to assay for electrostatic properties of nanoscale DNA-CNT hybrids. More specifically, we found that the outcome of anion exchange-based DNA-CNT separation, as measured by optical absorption spectral changes from fraction to fraction, is strongly dependent on the DNA sequence. To explore this dependence, we conducted a systematic but limited search of the huge ssDNA library under identical chromatographic conditions. The CNT dispersion procedure is a slight modification of that reported before (6). We found that sonication (i.e., disruption with sonic waves) effectively cuts CNTs in the presence of DNA and that short CNTs increase sample recovery from an anion exchange column. In a typical dispersion experiment, a DNA-CNT mixture was kept in an ice-water bath and sonicated (Sonics, VC130 PB, Newton, CT) for 120 min at a power level of 8 W. The average length of CNTs after this level of sonication is ~140 nm, as measured by atomic force microscopy (AFM). CNTs were “as produced HiPco (high pressure CO)” type from Carbon Nanotechnologies Inc. (Houston, TX), and DNAs were custom-made by Integrated DNA technologies, Inc. (Coralville, IA). We tested simple homopolymers of dA (deoxyadenylate), dC (deoxycytidylate), and dT (deoxythymidylate), as well as sub-libraries composed of totally random combinations of two of the four nucleotides [dG (deoxyguanylate), dA, dT, dC]: poly d(A/C), poly d(A/G), poly d(A/T), poly d(C/T), poly d(C/G), and poly d(G/T). Among these, poly d(G/T) and poly d(G/C) showed the largest variation in the optical absorption spectra from fraction to fraction. To narrow down the choice

<sup>1</sup>DuPont Central Research and Development, Experimental Station, Wilmington, DE 19880, USA. <sup>2</sup>Department of Chemical and Biomolecular Engineering, University of Illinois at Urbana-Champaign, Urbana, IL 61801, USA. <sup>3</sup>Department of Physics, Electrical Engineering and Computer Science, Massachusetts Institute of Technology, Cambridge, MA 02139, USA.

\*To whom correspondence should be addressed. E-mail: ming.zheng@usa.dupont.com

†Permanent address: Centro de Desenvolvimento da Tecnologia Nuclear, CDTN/CNEN, Belo Horizonte-MG, 30123-970, Brazil.

## REPORTS

of sequence, we then tested representative sequences in the poly d(G/T) and poly d(G/C) sub-library. We found that the best separation was obtained with a sequence of repeats of alternating G and T, d(GT)<sub>n</sub>, with total length ranging from 20 to 90 bases ( $n = 10$  to 45). Figure 1 shows the elution profile of a d(GT)<sub>20</sub>-CNT solution from a strong anion exchange column. The first relatively narrow peak corresponds to free DNA, the second broad peak to DNA-CNT hybrids. The resolved features in the broad peak are indicative of an inhomogeneous population of species being fractionated.

Figure 2 shows the ultraviolet-visible-near infrared (UV-Vis-near IR) absorption spectra of fractionated DNA-CNTs. We take the systematic spectral change from early fractions to late fractions as direct evidence for structure-based CNT separation. Three regions are identified in Fig. 2, according to extensive studies reported in the literature for HiPco-type CNTs (12–14): first interband transitions for metals,  $M_{11}$  (400 to 650 nm), and first and second interband transitions for semiconductors,  $S_{11}$  (900 to 1600 nm) and  $S_{22}$  (550 to 900 nm), respectively. The starting material yielded a spectrum typical of singly dispersed CNTs in aqueous solution, with multiple peaks arising from different types of CNTs overlapping across the entire spectrum. In contrast, the spectrum from an early fraction f35 has only one major peak centered at 980 nm in the  $S_{11}$  region, corresponding to the  $S_{11}$  transition from the smallest diameter semiconducting tubes found in HiPco CNTs. Additionally  $M_{11}$  transitions are enhanced, indicating an enrichment in metallic tubes. The  $S_{11}$  region from later fractions (f36, f39, and f45) shows a systematic shift of intensity toward longer wavelength. Because, to a first approximation, the  $S_{11}$  transition wavelength is proportional to the tube diameter (2), the observed shift indicates a gradual increase in average semiconducting tube diameter from early to late fractions. There is also a simultaneous decrease in the  $M_{11}$  intensities in late fractions, corre-

sponding to a depletion of metallic tubes.

The overlapping transitions in the absorption spectra from different types of tubes can be resolved by resonance Raman spectroscopy, providing a means to monitor changes of individual CNT tube types in the separation process. Raman spectroscopy with six excitation wavelengths (457, 501.9, 514.5, 532, 633, and 785 nm) was used to probe the metallic and semiconducting nanotubes in each fraction. We focused on the Raman radial breathing mode, because it is a direct measure of tube diameter, in most cases allowing for the monitoring of a particular (n,m) nanotube during the separation process (15). This is aided by recent spectral assignments of metallic (14) and semiconducting (13) nanotubes. A total of 29 different types of tubes were resolved. Representative spectra are shown in Fig. 3, A and B, which plot the radial breathing mode region with excitation at 785 and 501.9 nm, resonating with a population of semiconducting and metallic nanotubes, respectively. These data show that from early to late fractions, there is a gradual increase in diameter for semiconducting tubes (Fig. 3A) and a gradual depletion of metallic tubes (Fig. 3B).

We developed a quantitative analysis for average tube diameter in each fraction based on Raman data. A nanotube feature of intensity  $I_{fn}$  in a fraction  $f_n$  can be normalized against its intensity  $I_{f0}$  in the starting material  $f_0$  by the ratio  $I_{fn}/I_{f0}$ , which gives the relative tube concentration in  $f_n$ . The average tube diameter in  $f_n$  can be defined as a normalized weighted sum over all  $N$  nanotubes probed at different Raman wavelengths, as follows

$$\langle d \rangle = \frac{\sum_{i=1}^N \left( \frac{I_{fn}}{I_{f0}} \right) f(d_i) d_i}{\sum_{i=1}^N \left( \frac{I_{fn}}{I_{f0}} \right) f(d_i)}$$

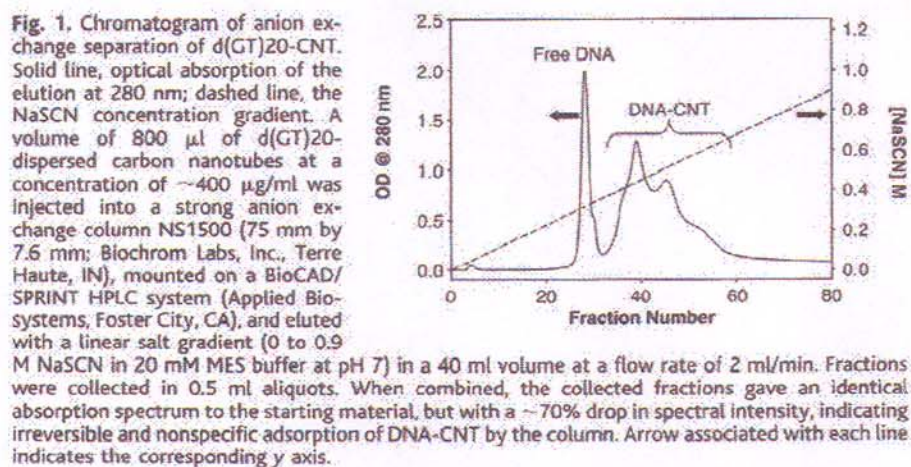


Fig. 1. Chromatogram of anion exchange separation of d(GT)<sub>20</sub>-CNT. Solid line, optical absorption of the elution at 280 nm; dashed line, the NaSCN concentration gradient. A volume of 800  $\mu$ l of d(GT)<sub>20</sub>-dispersed carbon nanotubes at a concentration of  $\sim$ 400  $\mu$ g/ml was injected into a strong anion exchange column NS1500 (75 mm by 7.6 mm; Biochrom Labs, Inc., Terre Haute, IN), mounted on a BioCAD/SPRINT HPLC system (Applied Biosystems, Foster City, CA), and eluted with a linear salt gradient (0 to 0.9 M NaSCN in 20 mM MES buffer at pH 7) in a 40 ml volume at a flow rate of 2 ml/min. Fractions were collected in 0.5 ml aliquots. When combined, the collected fractions gave an identical absorption spectrum to the starting material, but with a  $\sim$ 70% drop in spectral intensity, indicating irreversible and nonspecific adsorption of DNA-CNT by the column. Arrow associated with each line indicates the corresponding y axis.

where  $f(d)$  is the diameter distribution in the starting material and is modeled as a normal distribution with a mean diameter of 0.93 nm and a variance of 0.2 nm. This expression gives an average diameter of 0.93 nm for  $f_0$ , consistent with the model assumption, and gives 0.816 nm, 0.884 nm, 0.958 nm, and 1.084 nm for the semiconducting tubes in f35, f36, f40, and f45, respectively. An evaluation of the metal or semiconductor enrichment was also carried out based on resonance Raman measurements. Such an analysis showed that the content of metallic tubes drops from  $\sim$ 83% in early fractions (f36 and before) to  $\sim$ 10% in late fractions (f43 and after) (figs. S1 to S5).

Diameter-dependent separation allows fundamental studies of energy band structures of CNTs. Our preparative scale separation necessarily deconvolutes the first and second order interband transitions for semiconducting tubes, providing a clear mapping between these features for single nanotube types. By spectral fitting of the absorption spectra (Fig. 2) from the fractionated samples, we estimated that, over the diameter range explored in this work, the ratio of the E22 to E11 oscillator strengths is approximately 0.6.

To better understand the role of the d(GT)<sub>n</sub> sequence we chose for CNT separation, we used AFM to study its assembly on CNTs. Molecular modeling suggests that ssDNA can adopt many different modes of binding to CNTs, with little difference in binding free energies (6). These modes include helical wrapping with different pitches,

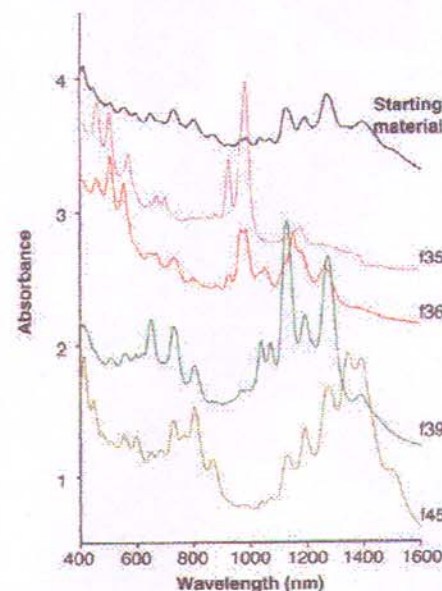


Fig. 2. Absorption spectroscopy on fractionated CNTs. Absorption spectra of the starting material (black), f35 (pink) (4X), f36 (red), f39 (green) (0.5 X), and f45 (olive green) from the experiment described in the text and Fig. 1.

consistent with our observations. In contrast,  $d(\text{GT})_n$  exhibits a qualitatively different binding to CNTs than most of the other ssDNA sequences. AFM measurements show

that  $d(\text{GT})_n$ -CNT hybrids have a much more uniform periodic structure with a regular pitch of  $\sim 18$  nm (Fig. 4A; figs. S6 S7). Whatever structure  $d(\text{GT})_n$  has on CNTs, it

appears to be very sensitive to minute changes in the structure of the nucleotide bases. Replacement of G or T by their homologs, inosine or uridine, respectively, decreases the degree of separation on the anion exchange column. Replacing  $d(\text{GT})_n$  with  $d(\text{GGTT})_{n/2}$  that has identical chemical composition also decreases the extent of the separation.

It is known that GT-rich sequences can self-assemble into supramolecular structures that play important roles in telomere replication (16), and GT-rich sequences have been observed to form nano-wires involving hydrogen-bonding interactions among different strands (17). As a model for the  $d(\text{GT})_n$ -CNT structure, we propose that two antiparallel  $d(\text{GT})_n$  strands interact with each other through hydrogen bonds to form a double-stranded strip (Fig. 4B), which then wraps around the CNT with close-packed bases resembling molecular tiles lying on the side wall of the nanotube (Fig. 4C). Such a double-helical structure is built on the unique hydrogen bonding network between two  $d(\text{GT})_n$  strands and is expected to be more rigid and to have fewer allowed conformations than a single-helical structure. A rigid DNA structure that creates an identical charge distribution within a given type of nanotube is necessary for successful separation. This is probably why most sequences disperse CNTs but do not give good separation.

The mechanism of separation can be explained by examining electrostatics of the DNA-CNT hybrid and its interaction with the positively charged substrate of the anion exchange resin. The DNA-CNT hybrid carries an effective negative charge because of the deprotonated backbone phosphate groups on the DNA (Fig. 4C). The interactions of the hybrid with the positively charged anion exchange resin and the eluting salt solution are electrostatic in nature, and they depend on linear charge density of the hybrid but not the length (18, 19). Indeed, AFM shows that different fractions have similar length distribution (50 to 500 nm). The effective net linear charge density of the hybrid material is determined first by the linear charge density of the phosphate groups along the nanotube axis. This value is modulated by differences in the electronic character of the nanotube core. For metallic tubes, the discrete negative charges on the DNA create along the tube axis an electrostatic field, which induces positive screening image charges (20) in the nanotube. As a result, the net linear charge density of the DNA-CNT hybrid is reduced from that of the DNA wrap alone. For semiconducting tubes, the lower polarizability of the nanotube, compared with that of the surrounding water, results in an increased effective lin-

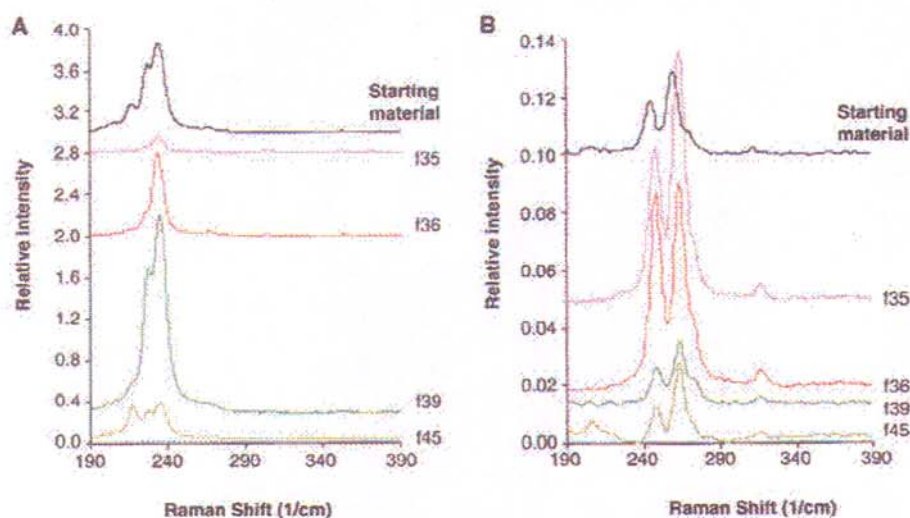


**Fig. 3.** Raman spectroscopy on fractionated CNTs. Colors are as in Fig. 2. (A) Raman spectra obtained using excitation at 785 nm, probing primarily semiconducting tubes. Early fractions show particular enhancement of smaller diameter nanotubes (larger Raman shift at  $305\text{ cm}^{-1}$  and  $354\text{ cm}^{-1}$ ). The opposite is observed for f45 (smaller Raman shift at  $218\text{ cm}^{-1}$ ). (B) Raman spectra obtained using 501.9 nm excitation, probing primarily metallic nanotubes. Fractions f35 and f36 show enhancement of these species.

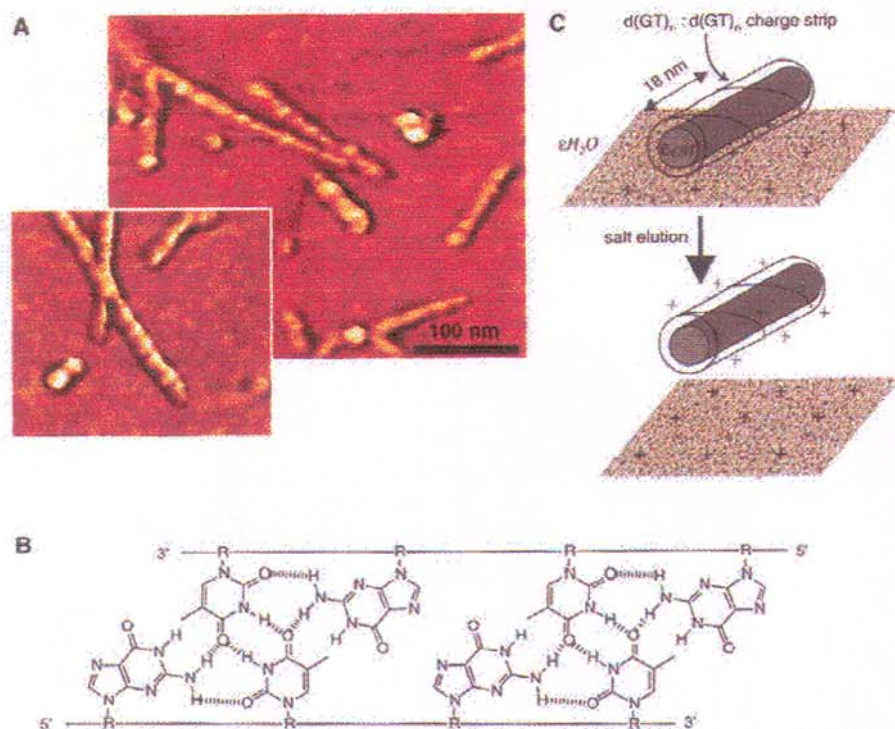


**Fig. 4.** Mechanism of DNA-CNT separation. (A) AFM (phase image) of CNTs wrapped by  $d(\text{GT})_{30}$ , showing regular helical pitch of  $\sim 18$  nm and height of  $\sim 2$  nm. (B) Proposed hydrogen-bonding interactions between two  $d(\text{GT})_n$  strands that lead to the formation of a "d(GT) $_n$ :d(GT) $_n$  charge strip." (C) Schematic for anion exchange separation process. At lower salt concentration, the surface-bound state is favored in which positive ions on the resin attract the negative surface charge on the DNA-CNT. With increasing salt concentration, the surface and DNA-CNT interactions are screened, favoring elution.

## REPORTS

ear charge density of the DNA-CNT hybrid relative to that of the DNA wrap alone, based on an image charge analysis for adjacent dielectrics (20). This fundamental difference in behavior provides ample differentiation between the binding strengths of metallic and semiconducting nanotubes to the anion exchange resin. Among semiconducting DNA-CNTs, there are two (nonexclusive) mechanisms that allow linear charge density to depend on tube diameter. First, because the polarizability of semiconducting nanotubes depends on diameter (21), the effective linear charge density is diameter-dependent. Second, the linear charge density of the DNA can change with tube diameter due to wrapping geometry changes. Together, these allow diameter-dependent separation of semiconducting tubes.

In summary, we have found that the attachment of ssDNA to a CNT is dependent on the specific DNA sequence and have shown

that this can form the basis for a method for CNT diameter and type separation.

### References and Notes

1. M. S. Dresselhaus, G. Dresselhaus, P. C. Eklund, *Science of Fullerenes and Carbon Nanotubes* (Academic Press, San Diego, CA, 1996).
2. R. Saito, G. Dresselhaus, M. S. Dresselhaus, *Physical Properties of Carbon Nanotubes* (Imperial College Press, London, 1998).
3. P. Avouris, *Acc. Chem. Res.* **35**, 1026 (2002).
4. S. Niyogi *et al.*, *Acc. Chem. Res.* **35**, 1105 (2002).
5. H. Dai, *Acc. Chem. Res.* **35**, 1035 (2002).
6. M. Zheng *et al.*, *Nature Mater.* **2**, 338 (2003).
7. D. Chattopadhyay, I. Galeska, F. A. Papadimitrakopoulos, *J. Am. Chem. Soc.* **125**, 3370 (2003).
8. R. Knipke, F. Hennrich, H. v. Lohneysen, M. M. Kappes, *Science* **301**, 344 (2003).
9. J. Liu *et al.*, *Science* **280**, 1253 (1998).
10. D. Chattopadhyay, S. Lastella, S. Kim, F. Papadimitrakopoulos, *J. Am. Chem. Soc.* **124**, 728 (2002).
11. S. K. Doorn *et al.*, *J. Am. Chem. Soc.* **124**, 3169 (2002).
12. M. J. O'Connell *et al.*, *Science* **297**, 593 (2002).
13. S. M. Bachilo *et al.*, *Science* **298**, 2361 (2002).
14. M. S. Strano *et al.*, *Nano Lett.* **3**, 1091 (2003).
15. J. L. Sauvajol *et al.*, *Carbon* **40**, 1697 (2002).
16. J. R. Williamson, *Annu. Rev. Biophys. Biomol. Struct.* **23**, 703 (1994).
17. T. C. Marsh, J. Vesenka, E. Henderson, *Nucleic Acids Res.* **23**, 696 (1995).
18. G. S. Manning, *Q. Rev. Biophys.* **2**, 179 (1978).
19. G. S. Manning, *Biophys. Chem.* **101-102**, 461 (2002).
20. J. D. Jackson, *Classical Electrodynamics* (John Wiley & Sons, New York, ed. 3, 1999).
21. L. X. Benedict, S. G. Louie, M. L. Cohen, *Phys. Rev. B* **52**, 8541 (1995).
22. This work comes from the Molecular Electronics group at DuPont CR&D. The DuPont group developed DNA-CNT hybrid materials and CNT separation strategy. The UIUC group and the MIT group independently conducted Raman spectroscopy analysis on fractionated CNT samples. A.P.S. acknowledges partial support from the Brazilian agency CNPq. M.S. acknowledges fundings from the National Science Foundation (grant CTS-0330350), the School of Chemical Sciences of the UIUC, and U.S. Department of Energy (award no. DEFG02-91ER45439).

### Supporting Online Material

[www.sciencemag.org/cgi/content/full/302/5650/1545/DC1](http://www.sciencemag.org/cgi/content/full/302/5650/1545/DC1)

DC1

SOM Text

Table S1

Figs. S1 to S7

References

25 September 2003; accepted 20 October 2003